Self-consistent treatment of electrostatics in molecular DNA braiding through external forces

Dominic J. Lee*
Department of Chemistry, Imperial College London, SW7 2AZ London, United Kingdom
(Received 4 April 2014; published 24 June 2014)

In this paper we consider a physical system in which two DNA molecules braid about each other. The distance between the two molecular ends, on either side of the braid, is held at a distance much larger than supercoiling radius of the braid. The system is subjected to an external pulling force, and a moment that induces the braiding. In a model, developed for understanding such a system, we assume that each molecule can be divided into a braided and unbraided section. We also suppose that the DNA is nicked so that there is no constraint of the individual linking numbers of the molecules. Included in the model are steric and electrostatic interactions, thermal fluctuations of the braided and unbraided sections of the molecule, as well as the constraint on the braid linking (catenation) number. We compare two approximations used in estimating the free energy of the braided section. One is where the amplitude of undulations of one molecule with respect to the other is determined only by steric interactions. The other is a self-consistent determination of the mean-squared amplitude of these undulations. In this second approximation electrostatics should play an important role in determining this quantity, as suggested by physical arguments. We see that if the electrostatic interaction is sufficiently large there are indeed notable differences between the two approximations. We go on to test the self-consistent approximation—included in the full model—against experimental data for such a system, and we find good agreement. However, there seems to be a slight left-right-handed braid asymmetry in some of the experimental results. We discuss what might be the origin of this small asymmetry.

DOI: 10.1103/PhysRevE.89.062711 PACS number(s): 87.80.Nj, 82.35.Pq, 87.10.Pq, 05.20.−y

I. INTRODUCTION

In biological systems DNA braiding occurs and has an important role to play. Two notable examples of DNA braiding are the formation of plectonemes and dual molecule catenanes. The former are a natural state for plasmids in bacteria [1], and plectonemes are also formed in the replication process [2] and in transcription [3] by the unraveling of the DNA strands. Catenane structures are seen between the two daughter DNA molecules as intermediates in the replication of a DNA plasmid [4,5].

In the past, to try to understand DNA braiding in plectonemes, single molecule twisting experiments have been performed [6–13]. However, only recently, has there also been an interest in performing dual braiding experiments [14–16], which may provide insights into braiding in DNA catenanelike structures. The experiments reported in Refs. [14,16] involve the two DNA molecules being attached by antibodies to a substrate and a magnetic bead. The magnetic field that is applied to the bead provides a pulling force that stretches out the DNA molecules, suppressing the undulations of the molecular center lines, and a moment that produces a fixed number of turns of the bead, and so a braid.

To describe single molecule twisting experiments and plectoneme supercoiling a considerable amount of theoretical work has been performed [17–29]. Most recent of these has been a study of multiplectoneme states that form in low salt concentrations [29]. For a dual molecular braid, a mathematical mechanical theory was constructed, in the ground state, describing the various braid structures formed by different combinations of mechanical forces on each molecule, with an additional interaction potential [30]; but, little work has been done on the statistical mechanics of dual molecular braiding [31,32]. However, in two recent publications [33,34], we have developed a model that describes braiding experiments of the form of those done in Ref. [16]. These models allow for the two ends of the two DNA molecules to be apart a distance much larger than the diameter of the braid that they form. This is relevant for the experiments of Ref. [16], as the DNA are attached to the bead with an end to end separation between the two molecules of the order of one micron. Also, one important improvement over the work of Ref. [32], is that we allow for a mean-field braid structure, which is self-consistently determined, that allows us to go to larger braid linking (catenation) numbers. We now allow for electrostatic interactions between molecules.

In the models of Refs. [33,34], the size of undulations of molecules, relative to each other, within the braid is determined only by steric interactions between the two molecules. However, when other interactions—for instance, electrostatic interactions—are present the size of these undulations should be self-consistently determined. There is a simple argument to suggest this. First, the size of undulations affects the average strength of intermolecular interactions. Therefore, if these interactions are repulsive, it is energetically unfavorable for molecules to have large amplitude undulations relative to each other. Thus, to reduce the free energy, the size of undulations will be reduced when repulsive interactions are indeed present. A self-consistent treatment of the amplitude undulations was originally pioneered in Ref. [24] for braids in plectonemes, and has been shown to fit the data of single molecule twisting experiments much better [28] than supposing that just steric interactions determine the mean-squared amplitude of undulations. With this in mind, we wanted to introduce a self-consistent determination of the mean-squared amplitude of such undulations into the theory. This treatment is along

*domolee@hotmail.com

similar lines to Ref. [24]; however, steric forces between the two molecules are also taken into account.

The work is presented in the following way. In the next section, we start by reviewing general features of the model, starting with the generic form we originally used in Refs. [33,34]. We then discuss the various contributions that we include in the free energy of the braided section of the two molecules. Next, a formula for the free energy of the braid is presented for the approximation used in Refs. [33,34]. Here, the mean-squared amplitude of undulations is determined only by steric interactions. We call this the simple approximation. Then, last of all, we present the form of the free energy, when the mean-squared amplitude of undulations is determined self-consistently from both electrostatic and steric interactions. The results section is divided into two parts. In the first part we compare the self-consistent approximation with the simple approximation, for different strengths of the electrostatic interaction between molecules. We show results for two geometric parameters that characterize the average structure of the braid as a function of the number of induced braid pitches. Also, we show the applied moment required to generate a particular number of braid turns (pitches) and the end to end extension of the two molecules. We see, indeed, as the strength of the electrostatic interaction is increased the difference between the two approximations increases. In the second part, we compare the self-consistent theory with experimental data from Ref. [16] and find good agreement with the model. In the last section, our discussion and outlook, we discuss extensions to the work, as well as the possibility that weak chiral interactions may account for the slight asymmetry between left- and right-handed braids seen in some of the experimental data.

II. MODEL

A. General considerations

In this paper we use a model, developed in Refs. [33,34], that describes braiding of two DNA molecules of identical length L, the value of which is assumed large enough for finite size effects not to be important. The two sets of molecular ends are held apart by distance b (see Fig. 1). One set of ends remains fixed, while the other set of ends is free to rotate about a common axis, which is assumed to be the axis of the braid (for a definition see below). To this system a pulling force F, in the direction along the braid axis, and a moment M that rotates the molecular ends about the same axis, are applied. In the model, we divide the DNA molecules into unbraided end pieces and a braided central section. This allows us to write the following free energy for our system:

$$\mathcal{F}_T = 2(L - L_b) f_{\mathrm{WLC}} + L_b f_{\mathrm{Braid}}, \tag{1}$$

where $2(L - L_b) f_{\mathrm{WLC}}$ is the contribution from the end pieces and $L_b f_{\mathrm{Braid}}$ is the contribution from the braided section. f_{Braid} will be taken to be a function of both M and F. As before [33,34], the four end pieces are assumed to behave like wormlike chains of contour length $(L - L_b)/2$, where L_b is the contour length of each of the two molecules that contributes to the braid.

Through the wormlike chain (WLC) model [35], it is possible to relate L_b to the parameters b, L, F, and $\frac{\eta_{\mathrm{end}}}{2}$ [33,34]; the last is the angle that both average molecular centerlines, of the end sections, make with the axis of the braid (see Fig. 1). This relationship reads as

$$L_b \approx \left\{ L - \left[1 + \left(\frac{k_B T \cos\left(\frac{\eta_{\mathrm{end}}}{2}\right)}{2 F l_p} \right)^{1/2} \right] \frac{b}{\left|\sin\left(\frac{\eta_{\mathrm{end}}}{2}\right)\right|} \right\} \times \theta \left(L - \left(1 + \left(\frac{k_B T \cos\left(\frac{\eta_{\mathrm{end}}}{2}\right)}{2 F l_p} \right)^{1/2} \right) \frac{b}{\left|\sin\left(\frac{\eta_{\mathrm{end}}}{2}\right)\right|} \right), \tag{2}$$

where $\theta(y)$ is the theta function, which for $y \geqslant 0$ is 1, otherwise zero, preventing a negative unphysical value of L_b. Here, l_p is the bending persistence length of the DNA molecules. For DNA we take the value $l_p \approx 500$ Å.

Followng Refs. [33,34], the free energy density of the end pieces is found to be

$$f_{\mathrm{WLC}}(b,F)(L - L_b) \approx -\frac{Fb}{2\left|\sin\left(\frac{\eta_{\mathrm{end}}}{2}\right)\right|} \left[\cos\left(\frac{\eta_{\mathrm{end}}}{2}\right) - \left(\frac{k_B T}{2 F l_p \cos\left(\frac{\eta_{\mathrm{end}}}{2}\right)} \right)^{1/2} \right]. \tag{3}$$

The total end to end distance of the two molecules is given by

$$z_T \approx \langle z_B \rangle + \sqrt{(L - L_b)^2 \left(1 - \sqrt{\frac{k_B T \cos(\eta_{\mathrm{end}}/2)}{F l_p}} \right)^2 - b^2}, \tag{4}$$

where the average length of the braid axis $\langle z_B \rangle$ (angular brackets will always correspond to thermal averaging) is determined from

$$\langle z_B \rangle = -L_b \frac{\partial f_{\mathrm{Braid}}(M,F)}{\partial F}. \tag{5}$$

It is useful to define the number of braid turns N as the (average) number of times the two molecules wrap around each other (number of pitches) in the braided section. This quantity is related to n through the relation

$$n \approx N + \frac{\mathrm{sgn}(n)}{2}, \tag{6}$$

where N is determined from

$$N = \frac{L_b}{2\pi} \frac{\partial f_{\mathrm{Braid}}}{\partial M}. \tag{7}$$

B. Braid geometry

For the thermally averaged structure of the braid, we assume that the two molecular center lines precess at a constant, and at the same, spatial frequency $\omega_{b,0}$ around a common axis that lies along the center of the braid; this axis is what we define as the braid axis. It is along and about this axis (when straight) F and M act, respectively. Equivalent positions along the

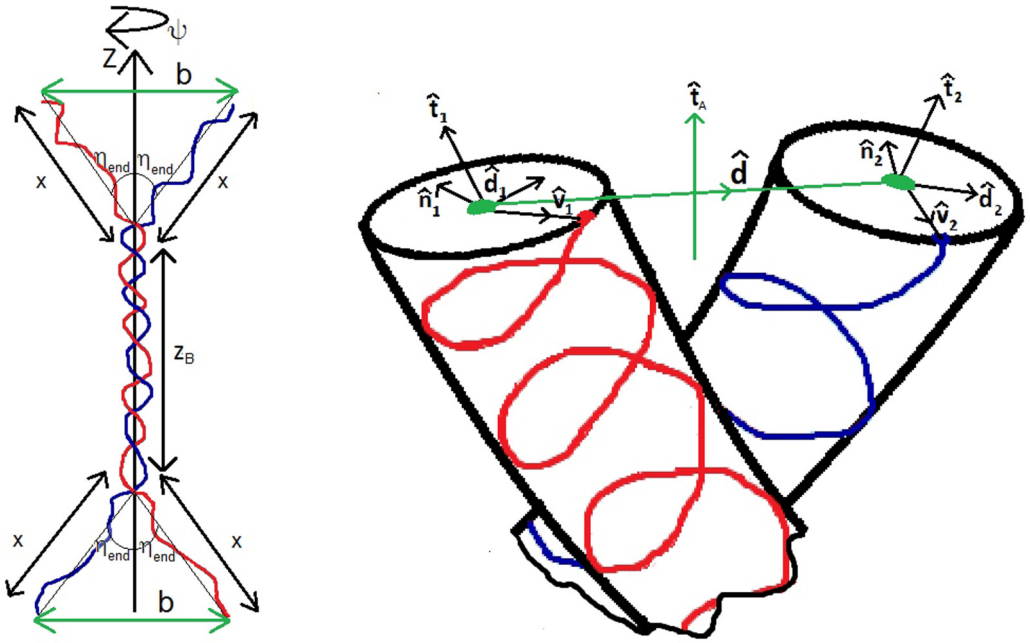

FIG. 1. (Color online) Schematic picture of the configuration of the two molecules. The left-hand picture shows the global configuration of two molecules. The red (lighter) line denotes one molecule, while the blue (darker) line denotes the other one. Both sets of molecular ends are separated distance b apart and one set of ends is rotated an angle ψ with respect to the other set about the axis of the braid. The distance x is the distance along the average position of the center lines of the end segments and is given by the WLC formula $x = (L - L_b)[1 - \sqrt{k_B T \cos(\eta_{\rm end}/2)/2l_p F}]$ (see Refs. [33,34]), where l_p is the bending persistence length of the two molecules. To generate this configuration, two of the ends may be attached to a magnetic bead and the other two ends to a substrate, as in the experiments of Ref. [16]. In the second picture we show the tangent vectors [$\hat{\mathbf{t}}_1(s)$ and $\hat{\mathbf{t}}_2(s)$] of the two molecular center lines, the vector $\hat{\mathbf{d}}(s)$ that lies along a line connecting the two molecular center lines [shown in green (light gray)], and the tangent vector of the braid center line that defines the local configuration of the braid. Also shown are the vectors $\hat{\mathbf{n}}_\mu(s)$ and $\hat{\mathbf{d}}_\mu(s)$ ($\mu = 1,2$), which are defined in Eqs. (8) and (9), that define the braid frames [30] of the two molecules. When $R'(s) = 0$ we have $\hat{\mathbf{d}}_1(s) = \hat{\mathbf{d}}_2(s) = \hat{\mathbf{d}}(s)$. The vectors $\hat{\mathbf{v}}_\mu(s)$ characterize the azimuthal orientation of the minor grooves of both molecules, the trajectories of which are shown by the two distorted helices in the right-hand side figure.

two molecular center lines may be described by an arclength coordinate s that runs from $-L_b/2$ to $L_b/2$. At any point along the braid, we may construct a line of length R that connects two points on the molecular center lines with the same arclength coordinate s. For the thermally averaged braid structure, $R(s) = R_0$ and is constant with respect to s. Indeed, the braid axis bisects the midpoint of this line. Pointing along this line is the unit vector $\hat{\mathbf{d}}(s)$, from which we may define unit vectors $\hat{\mathbf{d}}_1(s)$, $\hat{\mathbf{d}}_2(s)$, $\hat{\mathbf{n}}_1(s)$, and $\hat{\mathbf{n}}_2(s)$:

$$\hat{\mathbf{n}}_1(s) = \frac{\hat{\mathbf{t}}_1(s) \times \hat{\mathbf{d}}(s)}{|\hat{\mathbf{t}}_1(s) \times \hat{\mathbf{d}}(s)|}, \quad \hat{\mathbf{d}}_1(s) = \hat{\mathbf{n}}_1(s) \times \hat{\mathbf{t}}_1(s), \tag{8}$$

$$\hat{\mathbf{n}}_2(s) = \frac{\hat{\mathbf{t}}_2(s) \times \hat{\mathbf{d}}(s)}{|\hat{\mathbf{t}}_2(s) \times \hat{\mathbf{d}}(s)|}, \quad \hat{\mathbf{d}}_2(s) = \hat{\mathbf{n}}_2(s) \times \hat{\mathbf{t}}_2(s). \tag{9}$$

These vectors (shown in Fig. 1) define a "braid frame" [30], which can be used to characterize the local azimuthal orientations of the cross sections of the two molecules.

Also, to characterize the geometry of the braided section, we define a braid tilt angle $\eta(s)$. This is the angle between the two tangent vectors of the molecular center lines, $\hat{\mathbf{t}}_1(s)$ and $\hat{\mathbf{t}}_2(s)$, respectively, such that

$$\hat{\mathbf{t}}_1(s) \cdot \hat{\mathbf{t}}_2(s) = \cos\,\eta(s). \tag{10}$$

C. Description of the statistical mechanical model describing the braid

In the thermally averaged braid structure $\eta(s) = \eta_0$, the angle η_0 is assumed constant with respect to s, as it is related to the average frequency of precession $\omega_{b,0}$ of the two molecular center lines and R_0, which are constant. We allow for the braid to thermally fluctuate about this average structure by allowing for fluctuations in both η and R about the mean-field values η_0 and R_0. We also allow for small thermal undulations in the braid axis away from the configuration of a straight line. If the straight line configuration is supposed to lie on the z axis, fluctuations in the braid axis tangent vector may be characterized through $x'_A(s)$ and $y'_A(s)$; the derivatives of the displacements, away from the z axis in the x and y directions, respectively. All fluctuations in the local geometry depend on s. A particular configuration of the braid is assigned a Boltzmann weight in the partition function depending on its total energy. There are four contributing factors to the energy that we take account of, and thus in the free energy density $f_{\rm Braid}$.

The first is the bending elastic energy of the two molecules forming the braid, which is described by the elastic rod model for DNA. Here, the elastic energy is computed by integrating the sum of the squares of the curvatures, for both molecular center lines, along the lengths of the molecules contributing to the braided section and multiplying by $k_B T l_p/2$ (for expressions for the elastic energy contribution see Refs. [33,34]). The

second contribution is an electrostatic energy between helices [36] of the form

$$E_{\rm int} = \int_{-L_b/2}^{L_b/2} ds\{\mathcal{E}_{\rm dir}[R(s)] + \mathcal{E}_{\rm img}[R(s)]\}. \tag{11}$$

Here, $\mathcal{E}_{\rm img}[R(s)]$ is the contribution (a function of $R(s)$) from direct electrostatic interactions between the charges of one molecule and the other, and is given by

$$\frac{\mathcal{E}_{\rm dir}(R)}{k_BT} = \frac{2l_B(1-\theta)^2}{l_e^2}\frac{K_0(R\kappa_0)}{[a\kappa_0 K_1(a\kappa_0)]^2}. \tag{12}$$

The term $\mathcal{E}_{\rm img}[R(s)]$ is also repulsive, having effectively half the decay range. It is the contribution due to one molecule interacting with its image charge reflection at the surface of the other molecule (see Ref. [36]). It takes the form

$$\frac{\mathcal{E}_{\rm img}(R)}{k_BT} = -\frac{2l_B}{l_e^2}\sum_{n=-\infty}^{\infty}\sum_{j=-\infty}^{\infty}[\delta_{n,0}\theta - \cos(n\phi_s)]^2 \times \frac{K_{n-j}(R\kappa_n)K_{n-j}(R\kappa_n)}{[a\kappa_n K_n(a\kappa_n)]^2}\frac{I_j'(a\kappa_n)}{K_j'(a\kappa_n)}. \tag{13}$$

In Eqs. (12) and (13) we have

$$\kappa_n = \sqrt{\frac{1}{\lambda_D^2} + \left(\frac{2\pi n}{H}\right)^2}, \tag{14}$$

Where the Debye screening length is λ_D, the Bjerrum length is l_B (taken to be $l_B \approx 7$ Å), and the length is $l_e \approx 1.7$ Å, which is the inverse of the average DNA linear charge density (from only phosphate charges) multiplied by the unit charge e. The parameters a, ϕ_s, and H are the effective DNA radius (for electrostatics), the angular half width of the minor groove, and the average value of the DNA pitch. We choose the values $a \approx 11.2$ Å, $\phi_s \approx 0.4\pi$, and $H \approx 33.8$ Å. Equations (11)–(13) are a simplification of those used in Refs. [37,38,33], derived using the mean-field electrostatic model of Ref. [36] (for the most general calculation of the braid electrostatic energy, using the model of Ref. [36] see Ref. [39]). We have supposed, in Eqs. (11) and (12), that any forces depending on helix structure, in $\mathcal{E}_{\rm dir}(R)$, are completely washed out by thermal fluctuations (this corresponds to taking the limit $\lambda \to \infty$ in Eq. (9) of Ref. [33]). In this case, valid when helix specific forces are sufficiently weak, localizing ions near the DNA grooves has a small effect on the results. Furthermore, for monovalent salt ions (with the notable exception of some transition metals), we do not expect a large degree of localization [40]. Therefore, for simplicity, we suppose that the layer of condensed counterions is uniformly distributed near the DNA surface, compensating the bare DNA charge by a fraction θ. We will see that Eqs. (11)–(13) seem to adequately describe the electrostatic interaction in the monovalent salt experiments of Ref. [16]. Though, as a correction to Eq. (11), there may well be a weak residual chiral interaction from correlations between the helix structures of the two molecules that leads to a very slight $n \to -n$ asymmetry seen in some of the results of Ref. [16]. We will discuss this possibility later in the discussion section.

The third thing that we consider is steric interactions. Here, we assume that DNA molecules can be modeled as hard-core cylinders with steric radius a (see Refs. [38,41]). In treating the steric interaction, in the statistical mechanics, we use an approach originally developed in Ref. [42]. This is to replace the hard-core interaction with that of a harmonic potential with an effective spring constant $k_{\rm eff}$. This parameter depends on $R_0 - 2a$, which is a measure of the available space the molecules can fluctuate in, without colliding with each other. In the simple model, which we consider first, we assume the mean-squared amplitude of undulations is primarily determined by steric interactions such that

$$\langle (R - R_0)^2 \rangle \approx (R_0 - 2a)^2. \tag{15}$$

The requirement, Eq. (15), allows us to determine an approximate relationship between $k_{\rm eff}$ and $R_0 - 2a$ (see Refs. [38,34,41] for details) [43].

The last contribution is a work term that contains both the moment M and pulling force F which is of the form

$$E_W = -2\pi(Tw_b + Wr_b)M - z_B F, \tag{16}$$

where applying the external moment M changes the linking (catenation) number of the braid, $Lk_b = Tw_b + Wr_b$; the sum of braid twist and braid writhe, Tw_b and Wr_b, respectively. In Eq. (16) we do not constrain the linking numbers of the individual molecules as in Ref. [32], therefore considering the DNA molecules as nicked. The braid twist may be defined as

$$Tw_b = \frac{1}{2\pi}\int_{-L_A/2}^{L_A/2} d\tau\, \omega_b(\tau), \tag{17}$$

where $\omega_b(\tau)$ is the spatial frequency of precession of the center lines about the braid axis [note that $\langle \omega_b(\tau)\rangle = \omega_{b,0}$, and for an explicit expression of $\omega_b(\tau)$ in terms of the braid geometric parameters, see Ref. [41]]. The coordinate τ is of unit arclength along the braid axis, running from $-L_A/2$ to $L_A/2$ for the length of the braided section. The relationship between L_A and L_b depends on the configuration of the braid. In a configuration where the braid axis is straight $L_A = z_B$. The braid writhe is calculated through [44]

$$Wr_b = \frac{1}{4\pi}\int_{-L_A/2}^{L_A/2} d\tau \int_{-L_A/2}^{L_A/2} d\tau' \times \frac{[\mathbf{r}_A(\tau) - \mathbf{r}_A(\tau')]\cdot \hat{\mathbf{t}}_A(\tau)\times\hat{\mathbf{t}}_A(\tau')}{|\mathbf{r}_A(\tau) - \mathbf{r}_A(\tau')|^3}. \tag{18}$$

In Eq. (18), $\mathbf{r}_A(\tau)$ is the position vector that describes the trajectory of the braid axis and $\hat{\mathbf{t}}_A(\tau) = \frac{d\mathbf{r}_A(\tau)}{d\tau}$, the tangent vector. This decomposition of the braid linking number into braid twist and writhe for a molecular braid under tension was originally proposed in Ref. [32].

Strictly speaking, $Tw_b + Wr_b$ should be constrained to take exactly the value $-n + \mathrm{sgn}(n)/2$ (when $b \to \infty$). However, instead of working in an ensemble where $Tw_b + Wr_b$ is exactly fixed, we work in a fixed M ensemble, since it is much easier to do calculations. In the thermodynamic limit (the limit that we do our calculations in), where $L \to \infty$, these two ensembles are equivalent to each other. The fluctuations in the linking number in the fixed M ensemble become negligible in this limit [45]. Thus, through Eqs. (7) and (16), we have

in the thermodynamic limit $-N = \langle T w_b + W r_b \rangle$. In Refs. [34,41] explicit expressions for both z_B and $T w_b$ are given, but for brevity we do not give them here. In calculating the free energy, the term $2\pi M W r_b$ [in Eq. (16)] is considered to be small and is handled as a perturbation. This is done in a similar way to the theoretical calculations of Ref. [22], describing single molecule twisting experiments. In the calculations of Ref. [22], the writhe and twist are to do with the molecular center line and the trajectory of the minor groove (or some other point of reference that traces out the DNA double helix) about it.

D. The free energy in the simple approximation

Taking these contributions into account, following a variational approximation (the precise details of the calculation are given in Secs. 1–8 of Ref. [41]), we obtain the following form for the free energy:

$$\begin{aligned}\frac{f_{\rm Braid}}{k_BT} = &\left(\frac{F}{2l_pk_BT\cos\left(\frac{\eta_0}{2}\right)}\right)^{1/2} + \frac{\alpha_\eta^{1/2}}{2^{1/2}l_p^{1/2}} + \frac{1}{l_p^{1/3}}\frac{1}{2^{2/3}(R_0-2a)^{2/3}} - \frac{1}{R_0^2}\frac{l_p}{2^{1/3}}\left(\frac{R_0-2a}{l_p}\right)^{2/3}\sin^2\left(\frac{\eta_0}{2}\right)\\ &+ \frac{4l_p}{R_0^2}\sin^4\left(\frac{\eta_0}{2}\right) + \mathcal{E}_{\rm dir}(R_0) + \mathcal{E}_{\rm img}(R_0) - \frac{F}{k_BT}\cos\left(\frac{\eta_0}{2}\right) + \frac{2M}{k_BTR_0}\sin\left(\frac{\eta_0}{2}\right)\\ &- \frac{M}{4k_BTR_0}\frac{1}{2^{1/3}}\left(\frac{R_0-2a}{l_p}\right)^{2/3}\sin\left(\frac{\eta_0}{2}\right)^{-1} - \frac{M^2}{16l_p(k_BT)^2}\frac{1}{\cos\left(\frac{\eta_0}{2}\right)^{7/2}}\left(\frac{k_BT}{2Fl_p}\right)^{1/2},\end{aligned} \tag{19}$$

where

$$\alpha_\eta = \frac{4l_p}{R_0^2}\left[3\cos^2\left(\frac{\eta_0}{2}\right)\sin^2\left(\frac{\eta_0}{2}\right) - \sin^4\left(\frac{\eta_0}{2}\right)\right] + \frac{F}{4k_BT}\cos\left(\frac{\eta_0}{2}\right) - \frac{M}{2R_0k_BT}\sin\left(\frac{\eta_0}{2}\right). \tag{20}$$

In writing Eq. (19), we have further assumed that the thermally averaged bending energy terms and electrostatic energy can be replaced with their unaveraged values at R_0. The first term in Eq. (19) is the free energy contribution due to undulations of the braid axis. The entropic contribution due to fluctuations in η is given by the second term of Eq. (19). The third term is the contribution due to steric interactions between the molecules, in the braid, and the entropy loss of confining the molecules in a braided configuration of radius R_0. The next two terms are contributions from the bending elastic energy of the molecules in the braid. Next in Eq. (19), we have the contribution to the free energy from the electrostatic terms, which is simply given by $\mathcal{E}_{\rm dir}(R_0) + \mathcal{E}_{\rm img}(R_0)$. The next three terms are the contributions from $-z_BF - 2\pi T w_b M$ in the work term described by Eq. (16). The last term is the leading order nonvanishing contribution in the perturbation series in $-2\pi W r_b M$ (see Ref. [41]). The $\cos(\eta_0/2)$ terms, in this last term, arise from the fact that unit arclength of the braid axis, τ, should be used in computing the braid writhe, not the arclengths of the molecular center lines [see Eq. (18)]. Exactly the same M^2 term [in the limit $\cos(\eta_0/2) \to 1$] was also computed in Ref. [32] in the case where the average linking number of each molecule is left unconstrained (note that in Ref. [32] one should set $F = 2f$). However, the whole approach goes beyond that of Ref. [32] in two regards. We include the confinement through steric interactions of $\delta R(s)$, fluctuations in the relative distance between the two center lines, as well as considering fluctuations around a braided mean-field configuration.

Equations that determine both R_0 and η_0 are then found through the minimization conditions

$$\frac{df_{\rm Braid}}{dR_0} = 0 \quad \text{and} \quad \frac{df_{\rm Braid}}{d\eta_0} = 0. \tag{21}$$

Also, both $\langle z_B \rangle$ and N are related to F and M through Eqs. (5) and (7). By minimizing the total free energy, given by Eq. (1), with respect to $\eta_{\rm end}$ we find that for sufficiently large pulling force

$$\cos\left(\frac{\eta_{\rm end}}{2}\right) \approx -\frac{F}{f_{\rm Braid}} - \left(\frac{2k_BT}{Fl_p}\right)^{1/2}\left(-\frac{F}{f_{\rm Braid}}\right)^{3/2}. \tag{22}$$

E. Self-consistent determination of the mean-squared amplitude of undulations of the braid

In the case where there are just steric interactions, to maximize the entropy due to undulations, we simply have $\langle (R-R_0)^2 \rangle \approx (R_0-2a)^2$. However, when we have repulsive electrostatic interactions, undulations enhance the strength of their thermal average, making large undulations energetically unfavorable. Therefore, the electrostatic interaction should also limit the size of $\langle (R-R_0)^2 \rangle$. Therefore, it seems that a better approach is to set $\langle (R-R_0)^2 \rangle \approx d_R^2$, where d_R is self-consistently determined, primarily by electrostatic interactions, as well as steric forces. We also determine $\theta_R^2 = \langle (\frac{dR}{ds})^2 \rangle$ self-consistently.

In our expression for the free energy function we now use thermal averages of the bending energy and electrostatic energy terms; these averages help to determine d_R and θ_R. We do this according to a procedure used in Refs. [34] (for details, see Ref. [41]) and [38]. The idea is to introduce cutoffs on the amplitude of fluctuations in R, which we call $d_{\rm min}$ and $d_{\rm max}$. These cutoffs are the minimum and maximum values that $\delta R = R - R_0$ can take due to steric interactions. If $\delta R < d_{\rm min}$ or $\delta R > d_{\rm max}$, the values of both the bending and electrostatic energies are unphysical, as the molecules in the braid would have interpenetrated. Therefore, to prevent these unphysical values entering into the averaging, when $\delta R < d_{\rm min}$ we replace δR with $d_{\rm min}$, and when $\delta R > d_{\rm max}$ we replace δR with $d_{\rm max}$. We assume the values $d_{\rm max} = -d_{\rm min} = R_0 - 2a$, which should

be adequate for the braids that we will study here, although a different choice might possibly be used for much more tightly wrapped braids (see Refs. [38,41]).

The parameters d_R and θ_R are treated as variational parameters that minimize the following free energy (which can be derived following the steps presented in Secs. 10–12 in Ref. [41]):

$$\begin{aligned}\frac{f_{\text{Braid}}}{k_BT} &= \left(\frac{F}{2l_pk_BT\,\cos(\eta_0/2)}\right)^{1/2} + \frac{\alpha_\eta^{1/2}}{2^{1/2}l_p^{1/2}} + \frac{d_R^2}{2^{8/3}(R_0-2a)^{8/3}l_p^{1/3}} + \frac{1}{4l_p\theta_R^2} + \frac{l_p\theta_R^4}{4d_R^2} - \frac{M^2}{16l_p(k_BT)^2}\left(\frac{k_BT}{2l_pF_R}\right)^{1/2}\frac{1}{\cos\left(\frac{\eta_0}{2}\right)^{7/2}} \\ &- \frac{\theta_R^2l_p}{R_0^2}\,\tilde{f}_1\,[R_0,d_R,R_0-2a,-(R_0-2a)]\sin^2\left(\frac{\eta_0}{2}\right) + \frac{2l_B(1-\theta)^2}{l_e^2(a\kappa_D)^2K_1(a\kappa_D)^2}\,g_0\,[\kappa_DR_0,\kappa_Dd_R,(R_0-2a)/d_R,-(R_0-2a)/d_R] \\ &- \frac{2l_B}{l_e^2}\sum_{n=-\infty}^{\infty}\frac{[\cos(n\phi_s)-\theta\delta_{n,0}]^2}{[\kappa_naK_n'(\kappa_na)]^2}\,g_{\text{img}}\,[n,\kappa_nR_0,\kappa_nd_R,(R_0-2a)/d_R,-(R_0-2a)/d_R;a] \\ &+ \frac{4l_p\tilde{f}_1\,[R_0,d_R,R_0-2a,-(R_0-2a)]}{R_0^2}\sin^4\left(\frac{\eta_0}{2}\right) - \frac{F}{k_BT}\cos\left(\frac{\eta_0}{2}\right) + \frac{2M}{k_BTR_0}\sin\left(\frac{\eta_0}{2}\right)\tilde{f}_2\,[R_0,d_R,R_0-2a,-(R_0-2a)] \\ &- \frac{M\theta_R^2}{4k_BT}\frac{\tilde{f}_2\,[R_0,d_R,R_0-2a,-(R_0-2a)]}{R_0}\sin\left(\frac{\eta_0}{2}\right)^{-1}, \end{aligned} \tag{23}$$

where now

$$\begin{aligned}\alpha_\eta = \frac{4l_p\tilde{f}_1\,[R_0,d_R,R_0-2a,-(R_0-2a)]}{R_0^2}\left[3\cos^2\left(\frac{\eta_0}{2}\right)\sin^2\left(\frac{\eta_0}{2}\right) - \sin^4\left(\frac{\eta_0}{2}\right)\right] + \frac{F}{4k_BT}\cos\left(\frac{\eta_0}{2}\right) \\ - \frac{M\tilde{f}_2\,[R_0,d_R,R_0-2a,-(R_0-2a)]}{2R_0k_BT}\sin\left(\frac{\eta_0}{2}\right).\end{aligned} \tag{24}$$

The functions $\tilde{f}_1[R_0,d_R,R_0-2a,-(R_0-2a)]$ and $\tilde{f}_2[R_0,d_R,R_0-2a,-(R_0-2a)]$ come about from now averaging the bending energy, and the functions $g_j[\kappa_DR_0,\kappa_Dd_R,(R_0-2a)/d_R-(R_0-2a)/d_R]$ and $g_{\text{img}}[n,\kappa_nR_0,\kappa_nd_R,(R_0-2a)/d_R,-(R_0-2a)/d_R;a]$ from averaging the electrostatic energy, over the fluctuations in $R(s)$. The forms of these functions are given in the Appendix, for the interested reader. As well as replacing the bending and electrostatic terms with their averages, there are also a couple of other important differences between Eqs. (19) and (23). One is that the third term in Eq. (23), the contribution from steric interactions, now depends on d_R as well as R_0-2a. Another is the appearance of two entropic terms, the fourth and fifth terms, that depend on θ_R and d_R, which want to maximize the latter quantity, while steric, bending and electrostatic terms want to restrict its value.

Equations on θ_R, d_R, R_0, and η_0 are now obtained through the conditions

$$\frac{\partial f_{\text{Braid}}}{\partial\theta_R}=0,\quad \frac{\partial f_{\text{Braid}}}{\partial d_R}=0,\quad \frac{\partial f_{\text{Braid}}}{\partial\eta_0}=0,\quad \text{and}\quad \frac{\partial f_{\text{Braid}}}{\partial R_0}=0. \tag{25}$$

We will look at the first condition in Eq. (25) in detail; the other equations can be generated by combining Eqs. (23) and (25), and general forms for them can be found in Ref. [41]. From this first condition we obtain the equation

$$\begin{aligned}0 = -\frac{1}{2l_p\theta_R^3} + \frac{l_p\theta_R^3}{d_R^2} - \frac{2\theta_Rl_p}{R_0^2}\tilde{f}_1[R_0,d_R,R_0-2a,-(R_0-2a)]\sin^2\left(\frac{\eta_0}{2}\right) \\ - \frac{M\theta_R}{2k_BT}\frac{\tilde{f}_2[R_0,d_R,R_0-2a,-(R_0-2a)]}{R_0}\sin\left(\frac{\eta_0}{2}\right)^{-1}.\end{aligned} \tag{26}$$

If we neglect the last two terms in Eq. (26), the contributions from the bending elastic energy and the work term, we simply recover an old result (see Ref. [38]):

$$\theta_R^2 = \frac{1}{2^{1/3}}\left(\frac{d_R}{l_p}\right)^{2/3}. \tag{27}$$

An important point to realize is that if we were to substitute Eq. (27) into Eq. (23) and replace the averages of the bending energy terms and electrostatic energy terms with their unaveraged values calculated at R_0, on minimization with respect to d_R, we would recover Eq. (19) for the free energy prior to minimization over R_0 and η_0. However, it is far more physically appropriate to consider the thermal averages of the bending energy and electrostatic interaction energy in the free energy.

In general we find that solution to Eq. (26) is well approximated by the formula

$$\theta_R \approx \left(\frac{d_R}{l_p}\right)^{1/3}\frac{1}{\left(4\Gamma^2+\frac{32}{9}\Gamma+2^{4/3}\right)^{1/8}}, \tag{28}$$

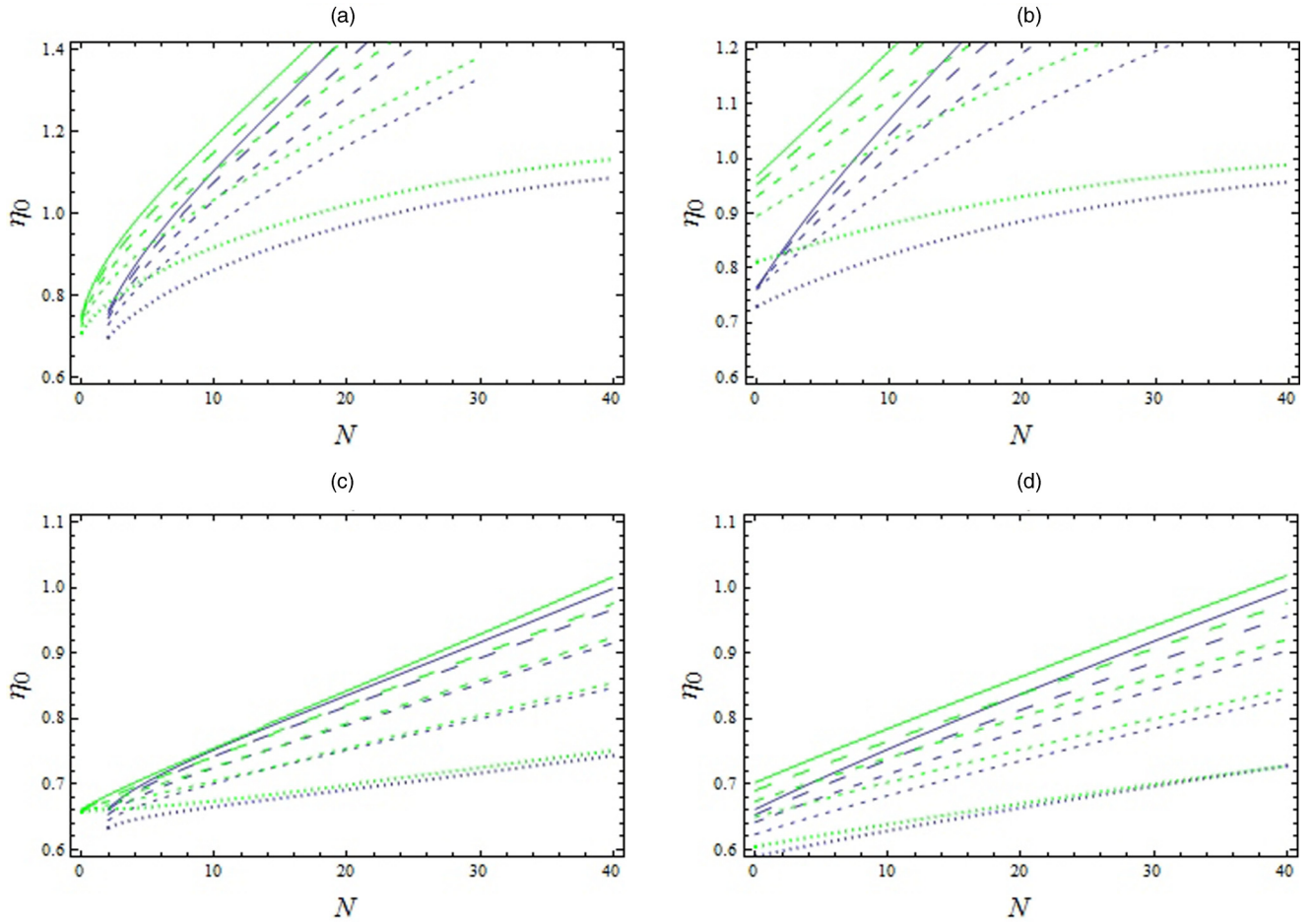

FIG. 2. (Color online) Graphs comparing the tilt angles calculated from the self-consistent treatment with those from the simple model. In all plots, the green (light gray) curves are generated using the simple model, while the blue (dark gray) curves are generated using the self-consistent treatment. In (a) and (b) we use a Debye screening length of $\lambda_D = 30.99$ Å, while in (c) and (d) $\lambda_D = 9.8$ Å is used. A pulling force of $F = 2$ pN is used in (a) and (c), and in (b) and (d) a pulling force of $F = 8$ pN is used. The solid, long-dashed, medium-dashed, short-dashed, and dotted-dashed lines correspond to values of $\theta = 0$, 0.2, 0.4, 0.6, and 0.8, respectively.

where

$$\Gamma = \left(\frac{d_R}{l_p}\right)^{4/3} \left\{ \frac{M l_p}{2R_0 k_B T} \tilde{f}_2[R_0, d_R, R_0 - 2a, -(R_0 - 2a)] \sin\left(\frac{\eta_0}{2}\right)^{-1} - \frac{2l_p^2}{R_0^2} \tilde{f}_1[R_0, d_R, R_0 - 2a, -(R_0 - 2a)] \sin^2\left(\frac{\eta_0}{2}\right) \right\}. \tag{29}$$

III. RESULTS

A. Comparing self-consistent treatment against simple model

Now, we compare the results obtained from Eqs. (19) and (21) with those obtained from Eqs. (23), (25), and (28). We examine the differences in η_0, R_0, M, and z_T as functions of N (the number of braid pitches) between the two approximations, for two pulling force values of $F = 2$ and 8 pN and Debye screening lengths $\lambda_D = 30.99$ and 9.8 Å, which roughly correspond to 1:1 monovalent salt concentrations of 10 and 100 mM, respectively.

In Fig. 2 we present plots for the average tilt angle. We see, generally, that the self-consistent approximation [using Eq. (23)] has a lower value of η_0 than the results determined from Eq. (19). This difference between the two approximations is most pronounced when $\lambda_D = 30.99$ Å. Also, the difference between the two approximations increases with the increase in the magnitude of the repulsive electrostatic interaction with decreasing θ. The difference can be accounted for in the following way. Averaging the bending energy terms, in the self-consistent treatment, as opposed to simply calculating them at R_0, enhances these terms, favoring a smaller value of η_0. The size of this enhancement is affected by d_R, which is in turn affected by R_0, as both electrostatic terms and bending terms help to determine d_R, as well as the steric interaction. As one reduces the value of θ and increases λ_D, one increases the value R_0, since one increases the electrostatic repulsion (see Fig. 3 below). This increase in R_0 has the tendency to increase d_R. Therefore, the difference is most pronounced for small θ and large λ_D. Also, we see that in all cases considered,

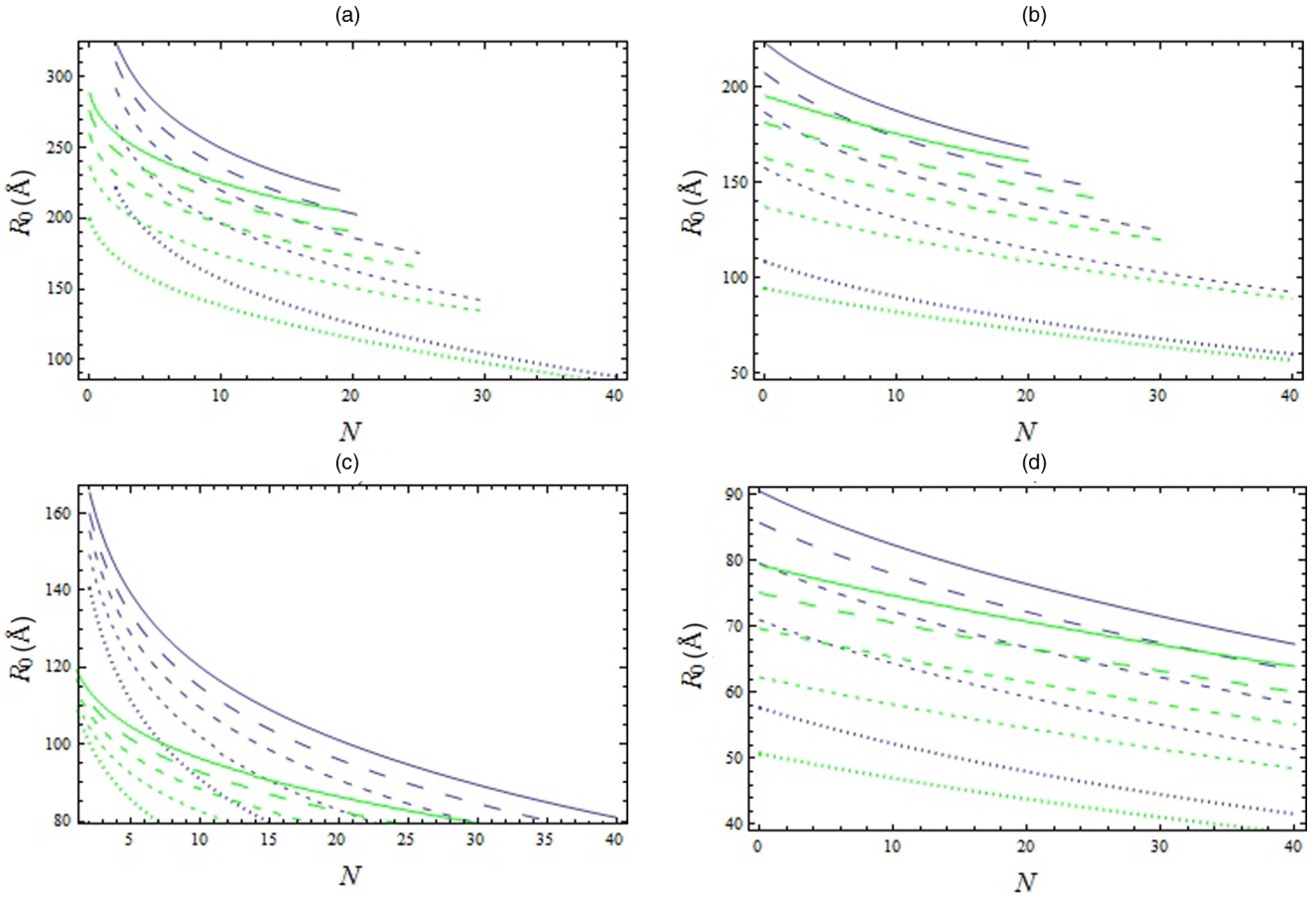

FIG. 3. (Color online) Graphs comparing the braid radius calculated from the self-consistent treatment with the simple model. In all plots, the green (light gray) curves are generated using the simple model, while the blue (dark gray) curves are generated using the self-consistent treatment. In (a) and (b) a Debye screening length of $\lambda_D = 30.99$ Å is used, while in (c) and (d) $\lambda_D = 9.8$ Å is used. A pulling force of $F = 2$ pN is used in (a) and (c), and in (b) and (d) a pulling force of $F = 8$ pN is used. The solid, long-dashed, medium-dashed, short-dashed, and dotted-dashed lines correspond to values of $\theta = 0$, 0.2, 0.4, 0.6, and 0.8, respectively. Note that in (a) and (b) some of the curves have been terminated, as η_{end} has become too large for the model to be valid.

reducing the value of θ and increasing λ_D both increase η_0. This is again attributable to the increase in R_0; here it weakens the bending energy terms in favor of the moment terms, which causes such an increase in η_0.

In Fig. 3 we present plots of R_0, as a function of the number of turns, for the two approximations. As we decrease θ and increase λ_D, we increase the amount of electrostatic repulsion in our system, which pushes up R_0. By increasing the pulling force F we reduce R_0 in the braid. This is because one requires a larger value of M to stabilize a braid; this larger value forces the two molecules closer together. We find that R_0 is always larger for the self-consistent approximation than for the simpler approximation. One reason for this increase, when we include undulations about R_0 into the electrostatic energy, is that this increases the amount of repulsion by enhancement of these terms. A second reason is an increase in the amount of repulsion due to entropy loss when confining the molecules to the braid, due to a reduction in $\langle \delta R(s)^2 \rangle$ when it is self-consistently calculated. The difference in R_0 between the two approximations is most pronounced at $\lambda_D = 9.81$. The explanation for this is that undulations enhance the electrostatics much more at $\lambda_D = 9.81$ than at $\lambda_D = 30.99$. This is due to the fractional increase in electrostatic energy, from reducing R, being much larger for the former case, so that the undulations about R_0 that reduce R strengthen the electrostatic interactions more here. Also, this difference between the two approximations is most pronounced at $F = 2$ pN and for small values of N; this is because at these values d_R is largest.

In Fig. 4 we examine the moment M as a function of the number of braid turns. The tendency, here, is for the self-consistent approximation to give a value of a slightly larger magnitude for the moment than for the simple approximation. At the low force value of $F = 2$ pN this difference is most apparent, especially for $\lambda_D = 9.8$ Å. This difference is due to the increase in electrostatic repulsion from the effect of averaging the electrostatic energy over the braid undulations, thereby increasing the amount of moment needed to do work against repulsive forces. These forces need to be overcome to bring the molecules close together, producing a braid of N turns.

Last of all, we compare the extensions in Fig. 5, or end to end distance z_T. In most plots, the self-consistent approximation gives a slightly larger value of z_T for fixed N. We might have expected the opposite (Ref. [33]), as for the self-consistent approximation we obtain a larger value of

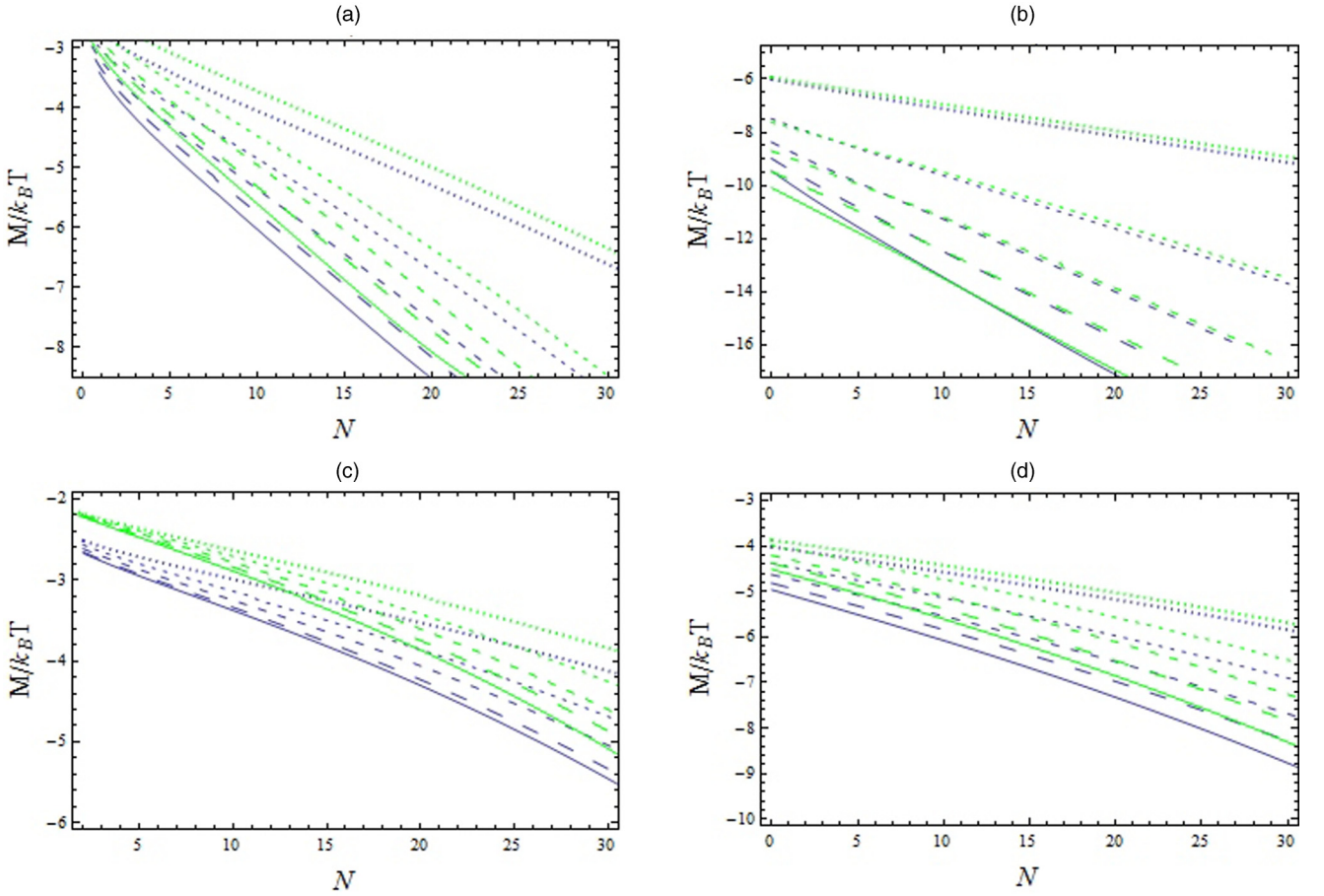

FIG. 4. (Color online) Graphs are shown comparing the relationship between the applied moment M and the number of braid turns, calculated from the self-consistent treatment with that from the simple model. In the calculations, the values $L = 36\,000$ Å and $b = 12\,000$ Å are used. The same color coding is used as in the previous figure. In (a) and (b) a Debye screening length of $\lambda_D = 30.99$ Å is used, while in (c) and (d) $\lambda_D = 9.8$ Å is used. A pulling force of $F = 2$ pN is used in (a) and (c), and in (b) and (d) a pulling force of $F = 8$ pN is used. The solid, long-dashed, medium-dashed, short-dashed, and dotted-dashed lines correspond to values of $\theta = 0$, 0.2, 0.4, 0.6, and 0.8, respectively. Note that all the moment curves have the symmetry property $M(N) = -M(-N)$.

R at fixed moment M, which would certainly be the case if η_0 and L_b remained fixed. However, the tilt angles η_0 are smaller for the self-consistent approximation than the simple approximation (see Fig. 2) as well as L_b. Also, we see that the differences between two approximations at $\lambda_D = 9.8$ Å seem to be very slight. Again, these differences, in most cases, are reduced with increasing θ, as we would expect.

B. Comparing self-consistent treatment against experimental data

We now match the self-consistent approximation with the experimental extension curves of Ref. [16]. We have essentially two fitting parameters b and θ; the former is a fitting parameter as it can only be determined from the extension data; it cannot be measured independently. Also, we should point out that the value of b cannot be controlled precisely in the experimental setup of Ref. [16], and may vary from one experiment to the next. One can fit b using only the extension data between $n = -1/2$ and $1/2$ where there is no braid. However, note, as was stated in Ref. [16], that there is a 10% error in the values of the measured applied pulling force F. Therefore, because of this and the fact that we do not have in all cases the available data, we fit b globally to the extension curves. Also due to this uncertainty in F we have used the generic value of $l_p \approx 500$ Å as opposed to a fine tuned value. It is also worth pointing out that l_p does vary slightly with salt concentrations between 10 and 100 mM [46].

To roughly quantify the goodness of the fit, we may compute a normalized variance for N_s experimental data points that lie in the region where the theoretical data curves are valid (i.e., $\eta_{\text{end}} \lesssim 1.8$ and $|n| > 1/2$). This is defined as

$$\sigma^2 = \sum_{j=1}^{N_s} \left[\frac{[z_T(n_j) - z_j]}{z_T(n_j)} \right]^2, \tag{30}$$

where for each experimental data point, we have the coordinates z_j and n_j for the extension and the number of bead turns. In Eq. (30), the theoretical curve is given by an interpolation function $z_T(n_j)$ generated from the numerical data. To obtain the best fit for b, we changed b in steps of 100 Å and computed σ^2 for each of the theoretical curves. For each value of θ, the value of b that generates $z_T(n)$ with the smallest value of σ^2 was judged to be the best fit.

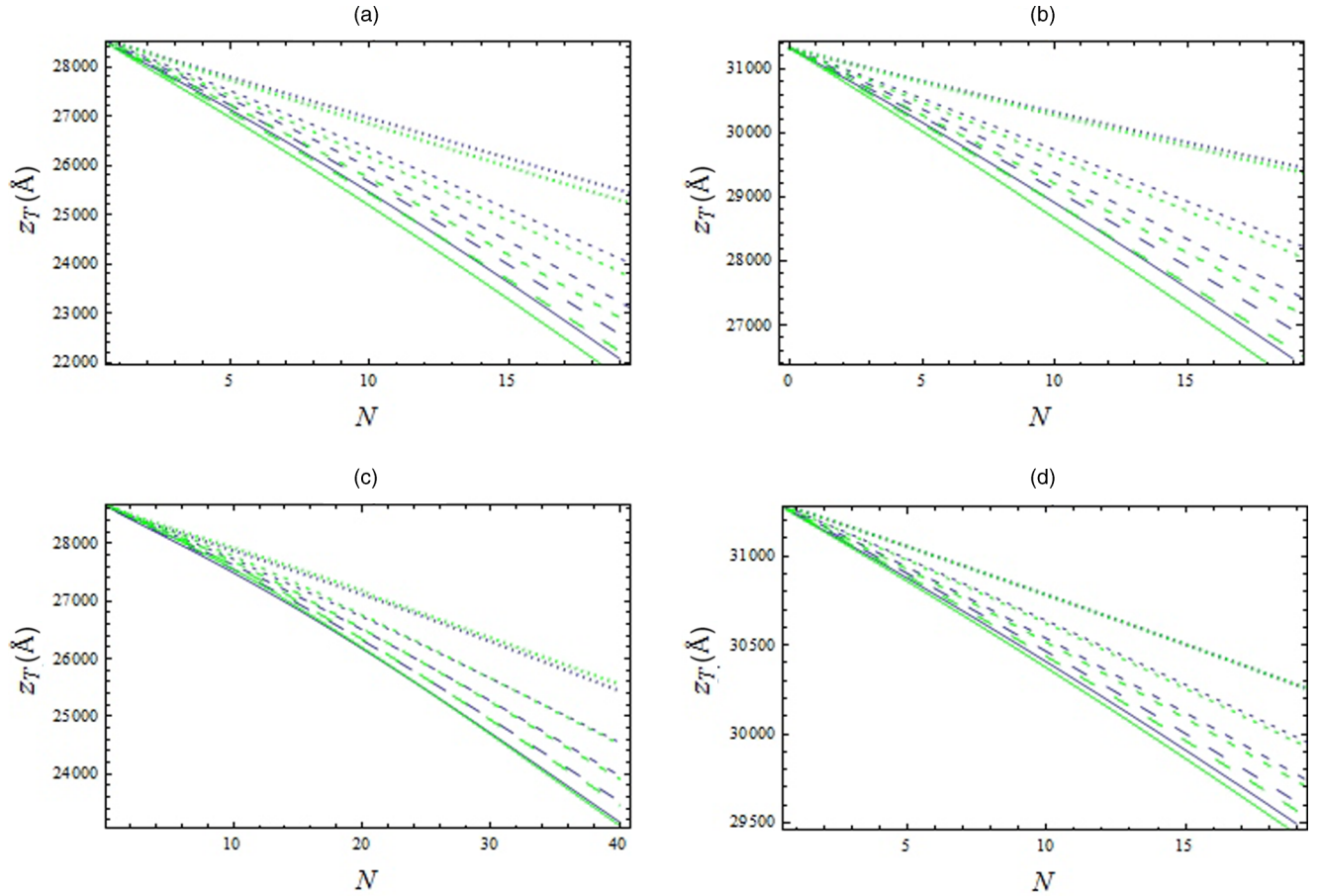

FIG. 5. (Color online) Graphs are shown comparing the extension z_T as a function of the number of braid turns calculated from the self-consistent treatment with the simple model. In the calculations, the values $L = 36\,000$ Å and $b = 12\,000$ Å are used. The same color coding is used as in the previous figure. In (a) and (b) a Debye screening length of $\lambda = 30.99$ Å is used, while in (c) and (d) $\lambda = 9.8$ Å is used. In (a) and (c) a pulling force of $F = 2$ pN is used, and in (b) and (d) a pulling force of $F = 8$ pN is used. The solid, long-dashed, medium-dashed, short-dashed, and dotted-dashed lines correspond to values of $\theta = 0$, 0.2, 0.4, 0.6, and 0.8, respectively. Note that the extension curves have the symmetry property $z_T(N) = z_T(-N)$.

We see that we can obtain good fits to the experimental data of Ref. [16] in Fig. 6. As we saw in Fig. 5 there may only be a slight difference in the extension curves between the two approximations. The improvement over the preliminary fits of Ref. [33], may in fact be mostly attributable to a slight difference in the expression for α_η and the additional term $\propto M^2$ in the free energy due to taking account of $-2\pi MWr_b$ in Eq. (16), the work term. However, there are significant differences in η_0, R_0, and M between the two approximations, and the self-consistent approximation reflects better physics.

Unfortunately, quite a large range of values of θ fit the extension curves for 100 and 10 mM, though with quite different fitted values of b (see Tables I and II). If the value of b was fixed, we would see the difference that is seen in Fig. 5, when changing θ, but some of this difference is offset by adjusting b. We find that for 10 mM the values $\theta = 0.5$ and $\theta = 0.6$ fit the data well (see Fig. 6), with the values of b given in Table I. The fits for $\theta = 0.4$ and $\theta = 0.7$ are significantly worse. For 100mM, we find that $\theta = 0.2$, 0.3 and 0.4 fit the data well; the best fit being $\theta = 0.2$. Again, all of these give different values of b (see Table II) and different curves for M as a function of n (see Fig. 6). We have refrained from going to $\theta = 0.1$, as we think this represents a rather unrealistic value of the charge compensation. All theoretical curves are terminated when roughly $\eta_{\text{end}} \approx 1.8$, as at this point buckling of the braid may have already occurred and the theory is not really strictly valid when $\eta_{\text{end}} > \pi/2$, although one can probably extrapolate slightly to our chosen value. The variances for the best fits to the 10 and 100 mM monovalent salt concentration data are given in Tables I and II, respectively.

IV. DISCUSSION AND OUTLOOK

In the results section, we started by comparing the self-consistent determination of the mean-squared amplitude of fluctuations with a cruder, but simpler, approach that was used in Refs. [33,34], and also implied in the calculations of Refs. [21,25,26,27,31,32]. This self-consistent calculation is akin to the approach used by Ref. [24] to describe the statistical mechanics of braiding, which was used successfully to match single molecule twisting data [28]. We found that there is a significant difference between the self-consistent approximation and the simpler approximation for η_0, R_0, and M, as functions of the number of braid turns, that grows

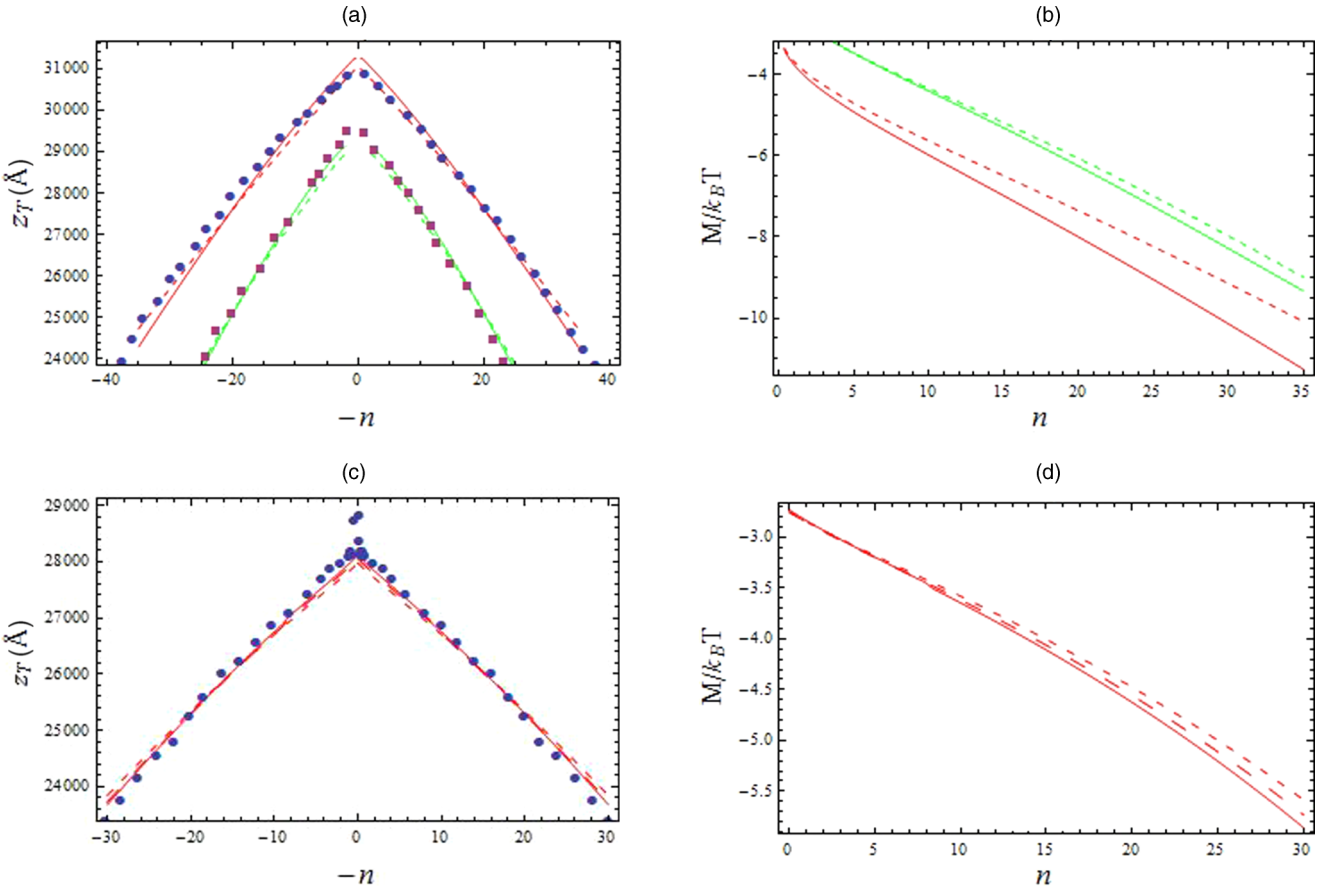

FIG. 6. (Color online) This figure shows the fits to the experimental extension curves along with the predicted applied moment for those fits. In (a) theoretical extension curves are fitted to experimental data from Ref. [16] at a monovalent salt concentration of 10 mM. The circles are experimental data for which a pulling force of $F = 4$ pN was used, whereas the squares correspond to a pulling force of $F = 2$ pN. The red (top) curves are theoretical curves calculated from the self-consistent approach at a pulling force of $F = 4$ pN, and the green (bottom) curves are theoretical curves calculated using $F = 2$ pN. For the solid lines a value of $\theta = 0.5$ was used and for the dashed curve a value of $\theta = 0.6$ was used. (b) shows the predicted applied moment for the fits to the 10 mM extension curve data, as a function of the number of turns of the bead, for the values $\theta = 0.5$ (shown by a solid line) and $\theta = 0.6$ (shown by a dashed line) at the force values $F = 2$ pN (higher curves, green) and $F = 4$ pN (lower curves, red). Note that the moment curves have the symmetry property $M(n) = -M(-n)$. In (c) we show fits of the experimental data of Ref. [16] at monovalent salt concentration 100 mM with pulling force $F = 2$ pN. The experimental data is given by circles, while the theoretical curves are given by the solid, long-dashed, and medium-dashed lines, corresponding to $\theta = 0.2,\ 0.3$, and 0.4, respectively. In (d) we show the predicted applied moment curves for the fits to the 100 mM extension data. Again, the solid, long-dashed, and medium-dashed lines correspond to $\theta = 0.2,\ 0.3$, and 0.4, respectively.

with the increasing strength of the electrostatic interaction. Though surprisingly, the difference between the two sets of extension curves is slight. Nevertheless, we would still advocate, unless the electrostatic interaction is particularly weak, that the self-consistent approximation is the better one to use, and it contains better physics.

To test this improved theory in describing the braiding of two molecules, we have fitted it against the experimental data

TABLE I. This table shows the fitted values of the distance b between the two sets of DNA ends (varied in steps of 100 Å) and normalized variance for the 10 mM monovalent salt data. The latter is calculated with Eq. (30), as a measure of how well each choice of θ fits the experimental data. Shown in the table are fits for the two pulling force values of $F = 2$ pN and $F = 4$ pN.

Charge compensation θ	Fitted value of b (Å)		Normalized variance squared of best fit	
	$F = 2$ pN	$F = 4$ pN	$F = 2$ pN	$F = 4$ pN
0.4	8400	7300	0.00 102	0.00 438
0.5	9100	8600	0.00 070	0.00 308
0.6	9900	9100	0.00 223	0.00 264
0.7	10 900	10 800	0.00 769	0.01 399

TABLE II. This table shows the fitted values of the distance b between the two sets of DNA ends (varied in steps of 100 Å) and normalized variance for the 100 mM monovalent salt data. The latter is calculated with Eq. (30), as a measure of how well each choice of θ fits the experimental data. Shown in the table are fits for the pulling force value of $F = 2$ pN.

Charge compensation θ	Fitted value of b (Å) $F = 2$ pN	Normalized variance Squared $F = 2$ pN
0.2	13 600	0.00 109
0.3	13 800	0.00 162
0.4	13 900	0.00 270
0.5	14 100	0.00 407

of Ref. [16], and have obtained good fits. However, we have not attempted to fit the force values $F = 0.5$ and 1 pN, as some of the approximations presented here are not quite valid for such low forces. Indeed, the expressions that are used to determine η_{end} [notably Eq. (22)] and Eqs. (2) and (3) are only valid at sufficiently large pulling force. Though, it is quite possible to extend the theory to these force values by numerically determining $\eta_{\text{end}}(F)$, $L_b(F)$, and $f_{\text{WLC}}(b, F)$ through the WLC model, but this has yet to be attempted. What is encouraging, in the current fits, is that the values of θ that fit the 10 mM data are larger than those that fit the 100 mM data. This is entirely consistent with the trend suggested by conventional counterion condensation theories, involving the solution of the nonlinear Poisson-Boltzmann equation, where the charge compensation should decrease from its Manning value [40], at infinite dilution, with increasing salt concentration. The values of $\theta \approx 0.2$–0.4 used to fit the 100 mM data are in line with the value of $\theta \approx 0.3$ used in Ref. [27] for 100 mM in single molecule twisting (corresponding to $\gamma = 1.44$ in Ref. [27]), based on the solution to the nonlinear Poisson-Boltzmann equation for a cylinder [47]. However, we should point out that the analysis of Ref. [48], suggests that the effective DNA charge should be reduced by an additional factor of 0.42 to fit experimental results for single molecule twisting better. This is presumably due to the role of DNA-DNA interactions in drawing more counterions close to the molecules. If this is the case, how much θ is increased should depend on the interaxial separation between molecules. Perhaps, in dual molecule braiding, the reason why the value of θ lies close to what Ref. [47] would predict is that R is quite large when the braid is formed at 2 pN (see Fig. 3). This suggests that over quite a large range of N the DNA-DNA interactions may not renormalize θ by that much. This might explain why we get a good fit to the experimental data, at a low value of θ. One possible way of refining the model would be to make the compensation parameter θ a function of both R and η, if such a function could be known from microscopic theory or simulation.

What is quite interesting is that there is a slight asymmetry in the experimental data, particularly seen for a 10 mM monovalent salt concentration, at a pulling force of $F = 4$ pN (cf. Fig. 6). As the molecules are nicked, and the molecules torsionally relaxed, this asymmetry cannot be explained by a difference in the twisting elastic response. Perhaps this slight asymmetry might be explained by weak correlations between the two helix structures of the braided part of the molecules. At any position along the braid, for a particular configuration of the molecules, we may write the following form for the interaction energy [39]:

$$\begin{aligned} E_{\text{int}} = & \int_{-L_b/2}^{L_b/2} ds\{\mathcal{E}_{\text{dir}}[R(s)] + \mathcal{E}_{\text{img}}[R(s)]\} \\ & + \int_{-L_b/2}^{L_b/2} ds\{\mathcal{A}_{1,\text{dir}}[R(s)] + \mathcal{B}_{1,\text{dir}}[R(s)] \sin\,\eta(s)\} \\ & \times \cos[\xi_1(s) - \xi_2(s)] \\ & + \int_{-L_b/2}^{L_b/2} ds\{\mathcal{A}_{2,\text{dir}}[R(s)] + \mathcal{B}_{2,\text{dir}}[R(s)] \sin\,\eta(s)\} \\ & \times \cos\{2[\xi_1(s) - \xi_2(s)]\}, \end{aligned} \tag{31}$$

where $\xi_1(s) = \hat{\mathbf{d}}_1(s) \cdot \hat{\mathbf{v}}_1(s)$ and $\xi_2(s) = \hat{\mathbf{d}}_2(s) \cdot \hat{\mathbf{v}}_2(s)$ are the azimuthal orientations of the minor grooves. The vectors $\hat{\mathbf{v}}_1(s)$ and $\hat{\mathbf{v}}_2(s)$ are perpendicular to $\hat{\mathbf{t}}_1(s)$ and $\hat{\mathbf{t}}_2(s)$, lying along lines connecting the molecular center lines with the minor grooves (shown in Fig. 1). The terms $\mathcal{A}_{j,\text{dir}}(R)$ and $\mathcal{B}_{j,\text{dir}}(R)$ are contributions to the direct electrostatic interaction, due to the helical structure of the molecules; the latter being terms that generate an internal chiral torque [33]. If the helix dependent second and third terms in Eq. (31) are sufficiently large, a preferred average azimuthal alignment $\langle \xi_1(s) - \xi_2(s) \rangle$ is maintained along the braid, and then the strong chiral regime discussed in Ref. [33] holds. However, if the terms are not quite large enough, $\langle \xi_1(s) - \xi_2(s) \rangle$ does not exist in the limit $L_b \to \infty$; there is no preferred average azimuthal orientation between the two grooves. Nevertheless, a term proportional in the free energy to $\sin\,\eta(s)$ (a chiral torque) is not completely washed out by thermal fluctuations in this state, as was originally suggested in Ref. [33]. While writing this paper, we realized that there is a possibility for weak transient correlations between $\xi_1(s)$ and $\xi_2(s)$ to occur in patches along the molecules, changing as the molecules thermally fluctuate, thereby causing a weak chiral torque. To calculate this weak chiral torque requires a different approach from the strong chiral interaction regime. In this new approach, the second and third terms in Eq. (31) should be treated as perturbations, when calculating the free energy. Such a perturbation approach was considered previously for DNA assemblies [49,50]. The leading order term of the perturbation expansion will still provide Eq. (23) [or Eq. (19)], but there should be a small correction to it from the perturbation expansion that breaks the $n \to -n$ symmetry. Indeed, we hope to look at this correction to the free energy, perhaps, in a later work to see whether it can account for the observed asymmetry. On the experimental side, if this is indeed the explanation for what is seen, we would expect the asymmetry becomes larger on increasing the force, as this brings the molecules closer, as well as by increasing the valance of the counterions, which should increase the relative strength of helix specific forces.

We still have yet to include buckling of the braid into the theory; when $|n|$ is sufficiently large, we would indeed expect it. In Fig. 6, we see a slight dip at both $n \approx 20$ and $n \approx -20$ in the 100 mM extension curve data. If this was experimental error, we would not expect that this dip would

occur on both sides of the extension curve of roughly the same value of n, perhaps suggesting a different explanation for this feature. Indeed, it is well known in single molecule twisting experiments [11–13] that on forming the end loop of a plectoneme the extension of the molecule drops in a discontinuous fashion. Interestingly, no such dip is seen in the 10 mM data of Ref. [16] (see Fig. 6). This actually is in line with theoretical [26,29] and experimental [11–13] trends for single molecule twisting; the size of the extension drop reduces and goes away with decreasing salt concentration. Therefore, perhaps this feature is indeed the hallmark of the formation of an end loop of a superplectoneme structure, in which the braid axis traces out a plectoneme. It may also be possible, in low salt concentrations, for multiple superplectonemes to form, rather like multiple plectoneme states form in single molecule twisting [29]. Though, it is also quite conceivable that it might be some other type of buckling, if it is not an experimental artifact. It would be interesting to see what a theory incorporating different buckled states would predict as the buckling transition and the type of buckling.

Recently, state of the art braiding experiments have been developed [51] using four optically trapped beads, which potentially offer much greater control over the geometry of the two molecules than those of Ref. [16], most notably b. Such experiments, perhaps, offer an opportunity to investigate DNA friction, the recent topic of a preliminary theoretical investigation [52]. In Ref. [52], the effect of the braid geometry was not taken into account; nevertheless it could be built upon using a similar framework to that suggested in Refs. [33,34], and this current work. However, a notable technical problem with these experiments is that, at present, only a few braid turns can be accommodated [53]. Therefore, the current model will need to be modified to the regime of a short braid to describe such experiments.

DNA micromanipulation experiments may also offer a unique tool to study the effects of DNA denaturing through agents such as viruses. In Ref. [54] it was shown what could be the response of the DNA with the introduction of particular virus capsids. It would be interesting to understand whether molecular braiding changes the double helix stability, through interactions between the molecules, affecting DNA denaturalization. By perhaps constructing suitable dual molecule braiding experiments, in the presence of denaturing agents, possible effects could be investigated. This might have some importance for DNA braiding in vivo.

At present, we are working on the possibility of the collapse of the braid into a tighter braided structure. Such a collapse may occur when there is a significant attractive component to the interaction between the two molecules. This might be caused by nonchiral attractive forces or forces dependent on helix structure. We hope to investigate both possibilities. For the latter, collapse into the tightly braided state happens predominantly in left-handed braids. Such a possibility has already been investigated and discussed in Ref. [33] in the strong chiral regime, but the extension curves, here, were calculated in the absence of molecular undulations in the braided section. However, we can now incorporate braid undulations [41]. We will also include an estimate of $\sin^2\eta(s)$ terms in the interaction energy, based on geometric arguments. From these arguments, the helical geometry of the DNA should actually limit the optimum value of the tilt angle $\eta(s)$, even in the absence of a bending rigidity term. In incorporating these two effects, we will see how the collapse of the braid for such forces is qualitatively changed from that of Ref. [33].

ACKNOWLEDGMENTS

D.J.L. would like to acknowledge useful discussions with R. Cortini, G. King, A. Korte, A. A. Korynshev, E. L. Starostin, G. H. M. van der Heijden, and G. J. L. Wuite. Additionally, he would also like to thank R. Cortini for providing him with experimental data. This work was initially inspired by joint work that has been supported by the United Kingdom Engineering and Physical Sciences Research Council (Grant No. EP/H004319/1). He would also like to acknowledge the support of the Human Frontiers Science Program (Grant No. RGP0049/2010-C102).

APPENDIX: FUNCTIONS APPEARING IN EQS. (23) AND (24)

Here, we give expressions of all the functions in the expression for the braid free energy [Eq. (23)] for the self-consistent calculation of the mean-squared amplitude of fluctuations in $R(s)$. These are

$$\tilde{f}_1(R_0,d_R,d_{\max},d_{\min}) = \frac{R_0^2}{d_R\sqrt{2\pi}}\int_{d_{\min}}^{d_{\max}}\frac{dx}{(R_0+x)^2}\exp\left(-\frac{x^2}{2d_R^2}\right) + \frac{1}{2}\left\{\frac{R_0^2}{(R_0+d_{\min})^2}\left[1-\operatorname{erf}\left(-\frac{d_{\min}}{d_R\sqrt{2}}\right)\right]+\frac{R_0^2}{(R_0+d_{\max})^2}\left[1-\operatorname{erf}\left(\frac{d_{\max}}{d_R\sqrt{2}}\right)\right]\right\}, \tag{A1}$$

$$\tilde{f}_2(R_0,d_R,d_{\max},d_{\min}) = \frac{R_0}{d_R\sqrt{2\pi}}\int_{d_{\min}}^{d_{\max}}\frac{dx}{(R_0+x)}\exp\left(-\frac{x^2}{2d_R^2}\right) + \frac{1}{2}\left\{\frac{R_0}{(R_0+d_{\min})}\left[1-\operatorname{erf}\left(-\frac{d_{\min}}{d_R\sqrt{2}}\right)\right]+\frac{R_0}{(R_0+d_{\max})}\left[1-\operatorname{erf}\left(\frac{d_{\max}}{d_R\sqrt{2}}\right)\right]\right\}, \tag{A2}$$

$$g_j(\kappa R_0,\kappa d_R,d_{\max}/d_R,d_{\min}/d_R) = \frac{1}{\sqrt{2\pi}}\int_{d_{\min}/d_R}^{d_{\max}/d_R} dy\, K_j(\kappa R_0 + y\kappa d_R)\exp\left(-\frac{y^2}{2}\right) + \frac{1}{2}K_j\left[\kappa(R_0+d_{\min})\right]\left[1-\operatorname{erf}\left(-\frac{1}{\sqrt{2}}\frac{d_{\min}}{d_R}\right)\right] + \frac{1}{2}K_j\left[\kappa(R_0+d_{\max})\right]\left[1-\operatorname{erf}\left(\frac{1}{\sqrt{2}}\frac{d_{\max}}{d_R}\right)\right], \tag{A3}$$

$$\begin{aligned} &g_{\mathrm{img}}(n,\kappa R_0,\kappa d_R,d_{\max}/d_R,d_{\min}/d_R;a) \\ &= \frac{1}{\sqrt{2\pi}}\sum_{j=-\infty}^{\infty}\int_{d_{\min}/d_R}^{d_{\max}/d_R} dy\, K_{n-j}(\kappa R_0 + y\kappa d_R)K_{n-j}(\kappa R_0 + y\kappa d_R)\frac{I_j'(\kappa a)}{K_j'(\kappa a)} \\ &\times \exp\left(-\frac{y^2}{2}\right) + \frac{1}{2}\sum_{j=-\infty}^{\infty} K_{n-j}[\kappa(R_0+d_{\min})]K_{n-j}\left[\kappa(R_0+d_{\min})\right]\frac{I_j'(\kappa a)}{K_j'(\kappa a)}\left[1-\operatorname{erf}\left(-\frac{1}{\sqrt{2}}\frac{d_{\min}}{d_R}\right)\right] \\ &+ \frac{1}{2}\sum_{j=-\infty}^{\infty} K_{n-j}[\kappa(R_0+d_{\max})]K_{n-j}\left[\kappa(R_0+d_{\max})\right]\frac{I_j'(\kappa a)}{K_j'(\kappa a)}\left[1-\operatorname{erf}\left(\frac{1}{\sqrt{2}}\frac{d_{\max}}{d_R}\right)\right]. \end{aligned} \tag{A4}$$

[1] V. A. Bloomfield, D. M. Crothers, and I. Tinoco, Jr., *Nucleic Acids, Structures, Properties, and Functions* (University Science Books, Sausalito, CA, 2000).
[2] J. C. Wang, Nat. Rev. Mol. Cell Biol. **3**, 430 (2002).
[3] L. F. Liu and J. C. Wang, Proc. Natl. Acad. Sci. U.S.A. **84**, 7024 (1987).
[4] S. D. Levene, C. Doanahue, T. Christian Boles, and N. R. Cozzarelli, Biophys. J. **69**, 1036 (1995).
[5] B. J. Peter, C. Ullsperger, H. Hiasa, K. J. Marians, and N. R. Cozzarelli, Cell **94**, 819 (1998).
[6] T. R. Strick, J. Allemand, D. Bensimon, A. Bensimon, and V. Croquette, Science **271**, 1835 (1996).
[7] P. Cluzel, A. Lebrun, C. Heller, R. Lavery, J.-L. Viovy, D. Chantenay, and F. Caron, Science **271**, 792 (1996).
[8] Z. Bryant, M. D. Stone, J. Gore, S. B. Smith, N. R. Cozzarelli, and C. Bustamente, Nature (London) **424**, 338 (2003).
[9] F. Mosconi, J. F. Allemand, D. Bensimon, and V. Croquette, Phys. Rev. Lett. **102**, 078301 (2009).
[10] Q. Shao, S. Goyal, L. Finzi, and D. Dunlap, Macromolecules **45**, 3188 (2012).
[11] H. Brutzer, N. Luzzietti, D. Klaue, and R. Seidel, Biophys. J. **98**, 1267 (2010).
[12] R. Schöpflin, H. Brutzer, O. Müller, R. Seidel, and G. Wedemann, Biophys. J. **103**, 323 (2012).
[13] S. Forth, C. Deufel, M. Y. Sheinin, B. Daniels, J. P. Sethna, and M. D. Wang, Phys. Rev. Lett. **100**, 148301 (2008).
[14] T. R. Strick, J.-F. Allemand, D. Bensimon, and V. Croquette, Biophys. J. **74**, 2016 (1998).
[15] M. D. Stone, Z. Bryant, N. J. Crisona, S. B. Smith, A. Vologodskii, C. Bustamante, and N. R. Cozzarelli, Proc. Natl. Acad. Sci. U.S.A. **100**, 8654 (2003).
[16] G. Charvin, A. Vologodskii, D. Bensimon, and V. Croquette, Biophys. J. **88**, 4124 (2005).
[17] F. Tanaka and H. Takahashi, J. Chem. Phys. **83**, 6017 (1985).
[18] B. D. Coleman and D. Swigon, J. Elast. **60**, 173 (2000).
[19] J. M. T. Thompson, G. H. M. van der Heijden, and S. Neukirch, Proc. R. Soc. London, Ser. A **458**, 1471 (2002).
[20] G. H. M. van der Heijden, J. M. T. Thompson, and S. Neukirch, J. Vib. Control **9**, 175 (2003).
[21] J. F. Marko and E. D. Siggia, Phys. Rev. E **52**, 2912 (1995).
[22] J. D. Moroz and P. Nelson, Proc. Natl. Acad. Sci. U.S.A. **94**, 14418 (1997).
[23] C. Bouchiat and M. Mezard, Phys. Rev. Lett. **80**, 1556 (1998).
[24] J. Ubbink and T. Odijk, Biophys. J. **76**, 2502 (1999).
[25] J. F. Marko, Phys. Rev. E **76**, 021926 (2007).
[26] J. F. Marko and S. Neukirch, Phys. Rev. E **85**, 011908 (2012).
[27] S. Neukirch and J. F. Marko, Phys. Rev. Lett. **106**, 138104 (2011).
[28] D. Argudo and P. K. Purohit, Acta Biomater. **8**, 2133 (2012).
[29] M. Emanuel, G. Lanzani, and H. Schiessel, Phys. Rev. E **88**, 022706 (2013).
[30] E. L. Starostin and G. H. M. Van der Heijden, J. Mech. Phys. Solids **64**, 83 (2014).
[31] J. F. Marko, Phys. Rev. E **55**, 1758 (1997).
[32] J. F. Marko, Phys. Rev. E **59**, 900 (1999).
[33] D. J. Lee, R. Cortini, A. Korte, E. Starostin, G. Van der Heijden, and A. A. Kornyshev, Soft Matter **9**, 9833 (2013).
[34] D. J. Lee, J. Phys.: Condens. Matter **26**, 245101 (2014).
[35] J. F. Marko and E. D. Siggia, Macromolecules **28**, 8759 (1995).
[36] A. A. Kornyshev and S. Leikin, J. Chem. Phys. **107**, 3656 (1997).
[37] R. Cortini, A. A. Kornyshev, D. J. Lee, and S. Leikin, Biophys. J. **101**, 875 (2011).
[38] D. J. Lee, Phys. Rev. E **88**, 022719 (2013).
[39] D. J. Lee, arXiv:1302.1420.
[40] A. A. Kornyshev, D. J. Lee, S. Leikin, and A. Wynveen, Rev. Mod. Phys. **79**, 943 (2007), and references contained therein.
[41] D. J. Lee, arXiv:1312.1568.
[42] W. Helfrich and W. Harbich, Chem. Scr. **25**, 32 (1985).
[43] It is worth mentioning that in the Gaussian chain model of two entwined directed polymers, the problem of steric interactions has been solved exactly [F. Ferrari, V. G. Rostiashvili, and T. A. Vilgis, Phys. Rev. E **71**, 061802 (2005)], assuming that the polymer diameter is negligible. Also, using a cylinder model for steric interactions an exact solution was obtained for the Gaussian model [R. Podgornik and V. A. Parsegian, Macromolecules **23**, 2265 (1990)]. However, for the wormlike

chain, things are rather more difficult due to the second derivative. Here, the resulting Schrödinger-like equation for the probability amplitude depends on both the direction of the tangent vector and the position of the molecular chain [H. J. Kleinert, J. Math. Phys. **27**, 3003 (1986)], and is generally difficult to solve.

[44] Strictly speaking from a mathematical perspective, this integral for the computation of writhe, as well as the definition of linking number, should be for a closed loop. However, one can think of a phantom chain that contributes to neither Lk_b nor Wr_b that connects the two ends of the braid to form a closed loop. Further justification of this extension to such non-closed-loop systems can be found in E. L. Starostin, *Physical and Numerical Models in Knot Theory Including Applications to the Life Sciences*, edited by J. A. Calvo, K. C. Millett, E. J. Rawdon, and A. Stasiak (World Scientific, Singapore, 2005), Chap. 26, pp. 525–545.

[45] Though the average braid axis is assumed to be straight [at least for small values of the fluctuations $x'_A(s)$ and $y'_A(s)$], the thermal average of the writhe is such that $\langle Wr_b \rangle \neq 0$. This is because of the presence of the term MWr_b in E_W [Eq. (16)]. This term prefers to induce coiling fluctuations of the braid axis of a preferred handedness, depending on the sign of M. However, provided that M is small, this imbalance due to MWr_b can be treated as a perturbation away from the straight axis braid configuration. This is indeed what we do, in calculating the free energy. However, if M becomes sufficiently high, we may expect a buckled braided state where $\langle Wr_b \rangle$ is substantial and we can no longer consider the average braid axis as being straight, but we do not consider such a state in our present study.

[46] C. G. Baumann, S. B. Smith, V. A. Bloomfirld, and C. Bustamante, Proc. Natl. Acad. Sci. U.S.A. **94**, 6185 (1997).

[47] D. Stigter, Colloid J. Interface Sci. **53**, 296 (1975).

[48] C. Maffeo, R. Schöpflin, H. Brutzer, R. Stehr, A. Aksimentiev, G. Wedemann, and R. Seidel, Phys. Rev. Lett. **105**, 158101 (2010).

[49] A. Wynveen, D. J. Lee, and A. A. Kornyshev, Eur. Phys. J. E **16**, 303 (2005).

[50] D. J. Lee and A. Wynveen, J. Phys.: Condens. Matter **18**, 787 (2006).

[51] M. C. Noom, B. van den Broek, J. van Mameren, and G. J. L. Wuite, Nat. Methods **4**, 1031 (2007).

[52] A. G. Cherstvy, J. Phys. Chem. B **113**, 5350 (2009).

[53] G. King (private communication); discussions with G. King and G. J. L. Wuite.

[54] J. Shin, A. G. Cherstvy, and R. Metzler, Phys. Rev. X **4**, 021002 (2014).